nature communications

Article

https://doi.org/10.1038/s41467-024-51213-z

RNA interactome of hypervirulent *Klebsiella pneumoniae* reveals a small RNA inhibitor of capsular mucoviscosity and virulence

Received: 26 April 2024

Accepted: 1 August 2024

Published online: 13 August 2024

Check for updates

Kejing Wu[1,6], Xingyu Lin[1,2,6], Yujie Lu[1,2,6], Rui Dong[1], Hongnian Jiang[1,2], Sarah L. Svensson[1], Jiajia Zheng[3], Ning Shen[3], Andrew Camilli[4] & Yanjie Chao[1,2,5]

Hypervirulent *Klebsiella pneumoniae* (HvKP) is an emerging bacterial pathogen causing invasive infection in immune-competent humans. The hypervirulence is strongly linked to the overproduction of hypermucoviscous capsule, but the underlying regulatory mechanisms of hypermucoviscosity (HMV) have been elusive, especially at the post-transcriptional level mediated by small noncoding RNAs (sRNAs). Using a recently developed RNA interactome profiling approach iRIL-seq, we interrogate the Hfq-associated sRNA regulatory network and establish an intracellular RNA-RNA interactome in HvKP. Our data reveal numerous interactions between sRNAs and HMV-related mRNAs, and identify a plethora of sRNAs that repress or promote HMV. One of the strongest HMV repressors is ArcZ, which is activated by the catabolite regulator CRP and targets many HMV-related genes including *mlaA* and *fbp*. We discover that MlaA and its function in phospholipid transport is crucial for capsule retention and HMV, inactivation of which abolishes *Klebsiella* virulence in mice. ArcZ overexpression drastically reduces bacterial burden in mice and reduces HMV in multiple hypervirulent and carbapenem-resistant clinical isolates, indicating ArcZ is a potent RNA inhibitor of bacterial pneumonia with therapeutic potential. Our work unravels a novel CRP-ArcZ-MlaA regulatory circuit of HMV and provides mechanistic insights into the post-transcriptional virulence control in a superbug of global concern.

The Gram-negative *Klebsiella pneumoniae* is an emerging bacterial pathogen in the era of global antibiotic crisis[1]. As a member of the ESKAPE pathogens, antibiotic-resistant *K. pneumoniae* is a leading cause of nosocomial infections and is difficult to treat by frontline drugs including carbapenems[2–4]. Whereas most classical *K. pneumoniae* strains affect immuno-deficient populations, a distinct pathotype of hypervirulent *K. pneumoniae* (HvKP) emerged in Asia in the 1980s that mainly infects young and healthy people, causing community-acquired pneumonia, liver abscess, endophthalmitis and meningitis[5–7]. More concerningly, HvKP can evolve to carbapenem-resistant (CR) strains via mobilizing plasmids, giving birth to CR-HvKP superbugs that are responsible for bursting endemics in China that pose urgent threats to global public health and biosecurity[8–11].

[1]Microbial RNA Systems Biology Unit, Center for Microbes, Development and Health (CMDH), Shanghai Institute of Immunity and Infection, Chinese Academy of Sciences, Shanghai, China. [2]University of Chinese Academy of Sciences, Beijing, China. [3]Center of Infectious Disease, Peking University Third Hospital, Beijing, China. [4]Department of Molecular Biology and Microbiology, Tufts University School of Medicine, Boston, MA, USA. [5]Key Laboratory of RNA Innovation, Science and Engineering (RISE), Shanghai Institute of Biochemistry and Cell Biology, Center for Excellence in Molecular Cell Science, Chinese Academy of Sciences, Shanghai, China. [6]These authors contributed equally: Kejing Wu, Xingyu Lin, Yujie Lu. e-mail: yjchao@ips.ac.cn

The virulence of HvKP is strongly linked to overproduction of capsular polysaccharides anchored to outer membrane[12]. With a limited number of recognized virulence traits such as lipopolysaccharide, fimbriae and siderophores, HvKP has been best characterized by its hypermucoviscosity (HMV) phenotype[13]. HvKP can form elastic strings longer than 5 mm when lifting their colonies from agar plates, a visible feature often used in clinical diagnosis[11]. HMV is largely attributed to copious capsule production and is required for invasive infections and pathogenesis[12]. The emergence of HMV has been associated with lateral acquisition of new capsule regulators[14,15], such as the *rmpADC* genes that promote capsule biosynthesis, transmembrane export, and chain extension[16–18]. Besides the capsule biosynthesis gene cluster, dozens of other genes have been found by global genetic screens to promote or suppress HMV (HMV-related genes), belonging to various pathways including central metabolism, iron homeostasis, RNA degradation, lipid transport, as well as global transcription factors such as CRP and OmpR[19–23]. Mounting evidence supports that HMV is tightly controlled at multiple layers by a complex regulatory network in *K. pneumoniae*.

Post-transcriptional control of HMV at the RNA level has been implicated in *K. pneumoniae*, but with little mechanistic understanding. For example, the major RNA chaperone Hfq has been shown to regulate capsule production and pathogenesis[24,25]. Hfq, as a conserved RNA-binding protein found in most bacteria, functions to stabilize small regulatory RNAs (sRNAs) and facilitate their base-pairing with target mRNAs (Fig. 1a)[26–28]. Hfq and its associated sRNAs regulate hundreds of mRNAs up to a quarter of the transcriptome in models such as *E. coli* and *Salmonella*, forming large post-transcriptional regulatory networks mediated by direct RNA-RNA interactions[29–33]. These RNA regulatory networks have been shown to control cell behaviors, stress responses, and metabolic fluxes in a wide range of bacterial pathogens including *S. enterica*, *Pseudomonas aeruginosa, Vibrio cholerae*, and *Clostridioides difficile*[34–40]. However, the nature and physiological function of this Hfq-mediated RNA network in the emerging hypervirulent pathotype of *K. pneumoniae* was little understood.

Here, we systematically profiled the RNA-RNA interactome of HvKP using an in vivo RNA proximity-ligation approach (iRIL-seq[34], Fig. 1a,) to decipher the RNA-mediated regulatory network. We discovered a plethora of Hfq-associated sRNA regulators of HMV and their interacting target mRNAs, establishing an intracellular RNA-RNA interactome map of HvKP and providing molecular insights into the role of post-transcriptional control in HMV. Our study revealed that the conserved enterobacterial sRNA ArcZ and its key targets are crucial regulators of HMV and *Klebsiella* pathogenesis in mouse models. ArcZ is transcriptionally activated by the master regulator of catabolite repression CRP, establishing a new link between central metabolism and HMV in *K. pneumoniae*.

Results

Hfq and Hfq-associated sRNAs regulate hypermucoviscosity in *K. pneumoniae*

Mucoid HvKP resists sedimentation by low-speed centrifugation (1000 *g*), and thus the OD_{600} of the supernatant from 1 OD of bacteria has been established as a quantitative readout for HMV[18,19]. Using this method, we first examined whether the major RNA chaperone Hfq and potentially sRNAs, might regulate HMV. Indeed, we observed a significant increase in supernatant OD values for a Δ*hfq* mutant at multiple growth stages (Fig. 1b, Supplementary Fig. 1), compared to the parental strain ATCC 43816 (serotype O1:K2), a well-known model HvKP strain used as wild-type throughout this study. As a negative control, the i-*wza* acapsular mutant, which carries a loss-of-function insertion in the capsule biosynthesis gene *wza*[19], was not mucoid and was pelleted completely by low-speed centrifugation. This result suggests that Hfq and Hfq-associated sRNAs may suppress HMV at the post-transcriptional level in HvKP.

iRIL-seq profiling of the RNA-RNA interactome in *K. pneumoniae*

To map the Hfq-mediated RNA regulatory network in HvKP, we harnessed the iRIL-seq approach recently established in our lab[34], which enables rapid profiling of intracellular RNA-RNA interactomes in live bacteria. Transformation of the pBAD-*t4rnl1* plasmid (pYC582) into *Klebsiella* allowed us to express T4 RNA ligase 1 for proximity-ligation of RNAs in vivo, followed by co-immunoprecipitation (coIP) to enrich the Hfq-bound RNA transcripts (singleton reads) and ligated RNA fragments (chimeras: sRNA-mRNA, sRNA-sRNA, etc) (Fig. 1a). The in vivo ligation followed by Hfq-FLAG-coIP (Hfq-coIP) was carried out in triplicate in cells at early stationary phase of growth in LB (OD_{600} of 3.0), with a monoclonal anti-FLAG antibody for IP and mouse IgG as a negative control (Fig. 1c). The resulting RNA samples were purified and subjected to Illumina paired-end sequencing (Supplementary Data 1).

Bioinformatic analysis of the sequencing reads confirmed a strong enrichment (>10-fold) of Hfq-associated sRNAs (singleton) in the Hfq-coIP samples over the IgG controls (Supplementary Fig. 2). 83 Hfq-associated sRNAs were detected in *K. pneumoniae*, including 43 sRNAs conserved in the Enterobacteriaceae family (including *E. coli* and *S. enterica*), as well as 40 novel sRNA candidates in *K. pneumoniae* (Supplementary Data 2). Hfq also directly bound to a large number of mRNAs. ~650 mRNAs (singleton) were enriched in our dataset >3-fold (Supplementary Data 3), indicating a large Hfq regulon exists in HvKP.

Ligation-derived chimeric fragments containing Hfq-associated sRNAs were also enriched by Hfq-coIP, occupying ~50% of all chimeric reads (Supplementary Fig. 2). We selected the significant chimeras (S-chimeras), defined as those with at least 10 reads and $p_{adj} < 0.05$ using the Fisher's exact test as previously reported[31,34], for subsequent analyses. The vast majority of S-chimeras (>90%) contained an sRNA at the 3′ half of chimera (RNA2), whereas the 5′ half (RNA1) comprised mostly mRNAs and sRNA fragments, which we consider binding partners of the sRNA (Fig. 1d). Under the condition analyzed here, eight sRNAs represented 90% of all singleton reads, whereas the ArcZ sRNA was highly enriched and ranked as the most abundant sRNA in S-chimeras (Fig. 1e).

Our analysis of the S-chimeras identified a total of ~2800 RNA-RNA interactions involving 76 sRNAs and 1264 target mRNAs, illustrating a large and complex RNA-RNA interaction network in HvKP (Fig. 1f). To better understand these interactions, we systematically analyzed the S-chimeras for sequence motifs. As expected, this analysis revealed a uridine stretch in the RNA2 portion at 3′ ends, consistent with rho-independent terminators found in most sRNAs (Fig. 1g). The RNA1 portion likely contains target mRNAs that basepair with the sRNA portion in RNA2[34]. Indeed, our analyses revealed many sequence motifs in RNA1 that show complementarity to the cognate sRNA in RNA2 (Fig. 1 h, i). In total, we identified significant sequence motifs for 15 sRNAs in S-chimeras (Supplementary Fig. 3), including several conserved enterobacterial primary (FnrS, MgrR, CyaR) and processed sRNAs (ArcZ, CpxQ, RprA), as well as a new *Klebsiella* sRNA candidate (KPnc0140). Complementary sequence motifs were discovered in over 90% of mRNA genes in RNA1 with the MAST $p < 0.001$, bolstering the high reliability of target identification using iRIL-seq analysis in vivo.

Members of the *Klebsiella* genus have relatively large genomes (>5 Mb) with a core genome similar to that of closely-related *E. coli* and *S. enterica*. iRIL-seq analysis in HvKP recapitulated many conserved RNA-RNA interactions previously reported in *E. coli* and *Salmonella* (Supplementary Data 4). For example, among 871 interactions involving ArcZ, we captured its orthologous target mRNAs including *tpx*, *sdaC*, and a sponge sRNA CyaR[32,41,42]. These sRNA-sRNA sponge interactions can titrate one or the other and inhibit their binding to target mRNAs[41]. In summary, the iRIL-seq analysis has established a comprehensive map of the RNA-RNA interactome in HvKP.

Multiple sRNAs regulate *Klebsiella* hypermucoviscosity

To identify potential sRNA regulators of HMV hinted at by our Δ*hfq* phenotype (Fig. 1b), we first inspected sRNA-mediated interactions

https://doi.org/10.1038/s41467-024-51213-z

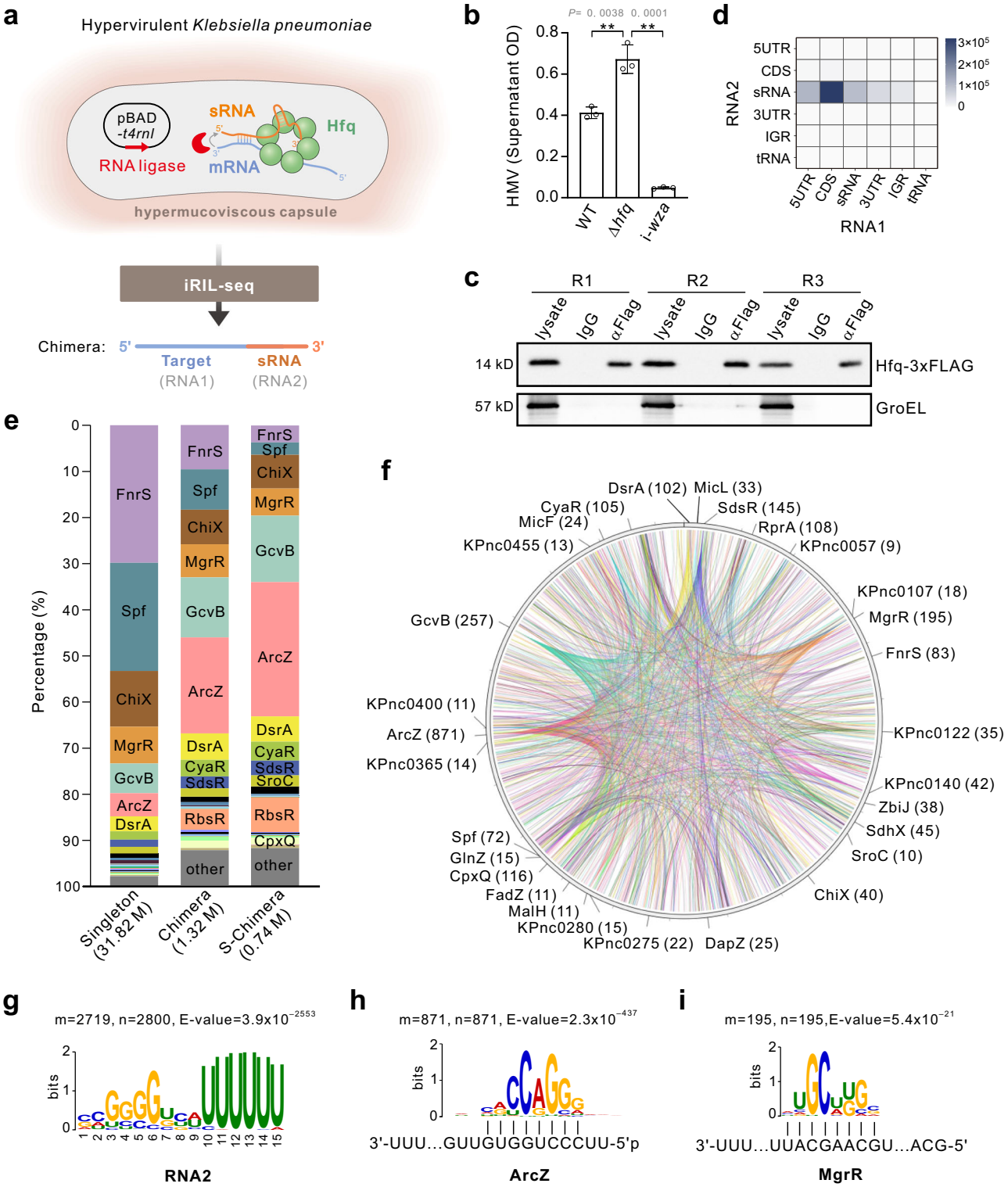

with the ~20 genes in the capsule biosynthesis cluster[18]. This revealed 21 sRNA candidates that may regulate HMV via interaction with up to 14 genes in the cluster (Fig. 2a). Outside the capsule locus, ~100 genes contributing to the HMV phenotype have been previously identified (Supplementary Data 5)[17–19,21]. Comparing the significant sRNA interactions against these HMV-related genes revealed another 27 sRNA candidates that may regulate HMV via interaction with 49 HMV-related genes (Fig. 2b). By combing both lists, our analysis revealed a large RNA regulatory network of HMV which involves a panel of 31 sRNAs and 64 mRNAs, providing a valuable resource for the study of post-transcriptional regulation of HMV in *K. pneumoniae* (Supplementary Data 6).

To experimentally validate these potential regulators of HMV, we cloned 23 sRNAs from the above list into the pZE12 vector and examined the impact of their overexpression on HMV in WT *Klebsiella*. While the pZE12 system is widely used to overexpress sRNAs in various bacteria[43], we found that it failed to overexpress ArcZ in *Klebsiella* (Supplementary Fig. 4). This is likely due to transcriptional repression of the P_{lacO} promoter by ~20 endogenous LacI-like repressors in the *Klebsiella* genome (Supplementary Fig. 5), and was overcome by a

Fig. 1 | iRIL-seq charts global RNA-RNA interactome in hypervirulent *K. pneumoniae*. **a** Schematic of in vivo RNA-RNA interactome profiling in HvKP. Interacting RNAs bound to Hfq are ligated by T4 RNA ligase 1, whose expression was induced from pBAD-*t4rnl1* (pYC582) in live *Klebsiella* cells. Hfq-bound transcripts (singleton) and ligated fragments (chimeras) are enriched by Hfq-coIP and analyzed by deep sequencing. **b** Hfq represses hypermucoviscosity. Overnight cultures were centrifuged at 1000 *g* for 5 min. The OD_{600} of the supernatant was determined and normalized to the OD_{600} of starting culture. The acapsular i-*wza* mutant serves as a non-mucoid control. $N = 3$ biological replicates, bars indicate mean ± SD. **, $p < 0.01$; two-tailed Student's *t*-test. **c** Western blot confirming Hfq pulldown. Strains carrying *hfq*–3xFLAG were grown to OD 3.0 and treated with 0.2% L-arabinose for 30 min. Lysates were subjected to coIP with anti-FLAG monoclonal antibody, or with mouse IgG as control. Lysates and IP samples are blotted using anti-FLAG, with GroEL as loading control. Image is representative of two experiments. Uncropped blots in Source Data. **d** Number of transcript types in significant chimeras (S-chimeras) for each combination of genomic elements. RNA1 and RNA2 constitute the 5′ portion and 3′ portion of a chimera, respectively. The numbers of interactions are indicated for each category in brackets. **e** Relative abundance of sRNAs detected in singleton and chimeric fragments. The percentage is obtained by dividing the number of fragments involving a given sRNA by the total fragments from sRNAs. The sRNA annotations are in Supplementary Data 2. **f** Circos plot showing the RNA-RNA interaction network in HvKP. Labeled sRNAs interact with >10 putative targets, and their interactions are shown in color. The number of interactions for each sRNA is indicated in brackets. A complete list of significant interactions is in Supplementary Data 4. Sequence motifs identified in RNA2 (**g**) and RNA1 (**h**, **i**) in S-chimeras. m, number of target sequences containing the motif; n, total number of target sequences. All motifs are in Supplementary Fig. 3.

supplementation of the culture with 1 mM IPTG (Supplementary Fig. 4a). Upon IPTG induction, most of the tested sRNAs showed a strong impact on HMV (Fig. 2c), corroborating the robustness of iRIL-seq analysis[34]. More than half (12/23) of the sRNAs tested reduced HMV vs. overexpression of a scrambled RNA in the control plasmid pJV300, whereas six sRNAs enhanced HMV to various degrees. ArcZ showed the strongest repression (~6-fold) of HMV in the presence of IPTG. Interestingly, HMV was also reduced by leaky expression of ArcZ in the absence of IPTG (Supplementary Fig. 4b), suggesting that HMV is highly sensitive to ArcZ levels.

Clinical *K. pneumoniae* strains are known for their extraordinary genetic diversity involving numerous sequence types and plasmid constituents[1]. To determine whether ArcZ repression of HMV is a conserved regulation or specific to our HvKP strain, we overexpressed ArcZ in a set of different HvKP clinical isolates (Supplementary Data 7). The results in Fig. 2d show that ArcZ induction significantly reduced HMV in all tested HvKP strains. These strains include another widely-used model strain NTUH-K2044[44], and a recent CR-HvKP clinical isolate (RJ9299) that is responsible for a local hospital outbreak in Shanghai, China[11]. These data strongly support that the regulation of HMV by ArcZ is a conserved mechanism among HvKP strains with diverse genetic backgrounds.

ArcZ is a conserved repressor of hypermucoviscosity

ArcZ was initially identified in *Salmonella* in the intergenic region between *arcB* and *elbB* (a.k.a. *yhbL*), and obtained its current name due to its partial overlap with *arcB*[42]. In *E. coli* and *Salmonella*, ArcZ is transcribed as a 129-nt long precursor sRNA (Pre-ArcZ) and further processed into the mature ArcZ sRNA[45,46]. In *K. pneumoniae*, the *arcZ* gene is located in the same intergenic region (Fig. 3a), and shares a conserved seed sequence with the other enterobacterial homologs (Fig. 3b). The primary sequence of Pre-ArcZ is identical in multiple *Klebsiella* type strains. Chromosomal deletion of *arcZ* led to significantly increases in HMV (Fig. 3c) and in the capsule amount (Fig. 3d). These increases in Δ*arcZ* were successfully complemented by introducing a single-copy of *arcZ* gene back in the chromosome at another locus. Therefore, the endogenous ArcZ sRNA represses the capsular HMV in *Klebsiella*, and likely acts in trans independent of its neighboring *arcB* gene (Supplementary Fig. 6).

According to our iRIL-seq data, ArcZ may directly interact with many mRNAs including several encoded in the capsule cluster or related to HMV (Fig. 3e, Supplementary Fig. 7). The expression levels of many capsule mRNAs were reduced when ArcZ was overexpressed (Supplementary Fig. 8). To understand the molecular mechanism how ArcZ regulates capsule and HMV, we selected several of these relevant genes and constructed translational GFP reporter fusions using the two-plasmid system[43]. Of eleven different target genes, ten (91%) were significantly repressed upon ArcZ overexpression ($p < 0.05$, Student's *t* test, Fig. 3f). The strongest suppression was observed for *mlaA* and *fbp*, two HMV-related genes located outside of the capsule cluster. MlaA is an outer-membrane lipoprotein that functions in the retrograde phospholipid trafficking pathway[47,48]. The *fbp* gene encodes fructose-1,6-bisphosphatase of the gluconeogenesis pathway[49]. Despite their involvement in different pathways, deletion of *mlaA* and *fbp* caused a significant reduction in HMV (Fig. 3g, h), mirroring the effect of ArcZ overexpression in *Klebsiella* (Fig. 2c, d).

To examine the regulation of MlaA and Fbp proteins in *Klebsiella*, we inserted chromosomal 3xFLAG tags at their respective C-termini and analyzed their levels by Western blotting. A clear upregulation (~1.7-fold) was observed for the MlaA-3xFLAG protein when *arcZ* was deleted (Fig. 3i), with little change for Fbp-3xFLAG (Fig. 3j). Overexpression of ArcZ strongly reduced both levels of MlaA and Fbp proteins (Fig. 3k, l). This inhibition was abolished by introducing 2- or 5-nt mutations into the conserved seed sequence of ArcZ (M2 and M5, Fig. 3b), suggesting a direct regulation involving the seed region of ArcZ.

ArcZ represses *mlaA* and *fbp* by direct basepairing interactions

ArcZ regulates the expression of *mlaA* and *fbp* likely via base-pairing with the mRNAs. Analysis of the iRIL-seq data revealed a large number of ArcZ chimeras mapped to the 5′UTRs of both *mlaA* and *fbp* mRNAs (Fig. 4 a, b), indicating that ArcZ basepairs at their 5′UTRs. Indeed, basepairing interactions were predicted, with both IntaRNA and RNAhybrid tools[50,51], between the conserved seed of ArcZ and the translation initiation region of both mRNAs (Fig. 4c, d). Using translational GFP reporters, we confirmed regulation of both targets at the post-transcriptional level. GFP fluorescence analysis showed that the target regulation requires the conserved seed region of ArcZ (Fig. 4e, f), consistent with Western blot results (Supplementary Fig. 9). Finally, introducing compensatory basepairing mutations in the target mRNAs (Fig. 4c, d), restored regulation by the ArcZ-M2 sRNA (Fig. 4e, f). These results show that ArcZ inhibits the translation of *mlaA* and *fbp* via direct RNA-RNA basepairing interactions.

ArcZ and MlaA are crucial for *Klebsiella* virulence

Given that HMV is a major virulence factor for *Klebsiella*, we next analyzed the role of ArcZ in virulence regulation using a murine infection model[52]. Compared to the WT strain, mice infected with the Δ*arcZ* mutant showed a trend of higher CFUs recovered from lung and spleen 48 h post-infection (Supplementary Fig. 10), without reaching statistical significance. Using a more sensitive competition assay with WT and Δ*arcZ* mixed together, we observed that Δ*arcZ* showed a significant competitive advantage over WT in mice (Fig. 5a), supporting that ArcZ is a repressor of *Klebsiella* virulence. In line with this observation, ArcZ expressed from its own promoter on multicopy plasmid (pZE12-P_{own}-*arcZ*) led to a significant reduction of *Klebsiella* load in lungs (Supplementary Fig. 10). Constitutive overexpression of ArcZ from a stronger 16 S rRNA promoter drastically reduced bacterial burden in mice by several orders of magnitude (Fig. 5b–d, Supplementary Fig. 11a). By stark contrast, no effect on bacterial load was

https://doi.org/10.1038/s41467-024-51213-z

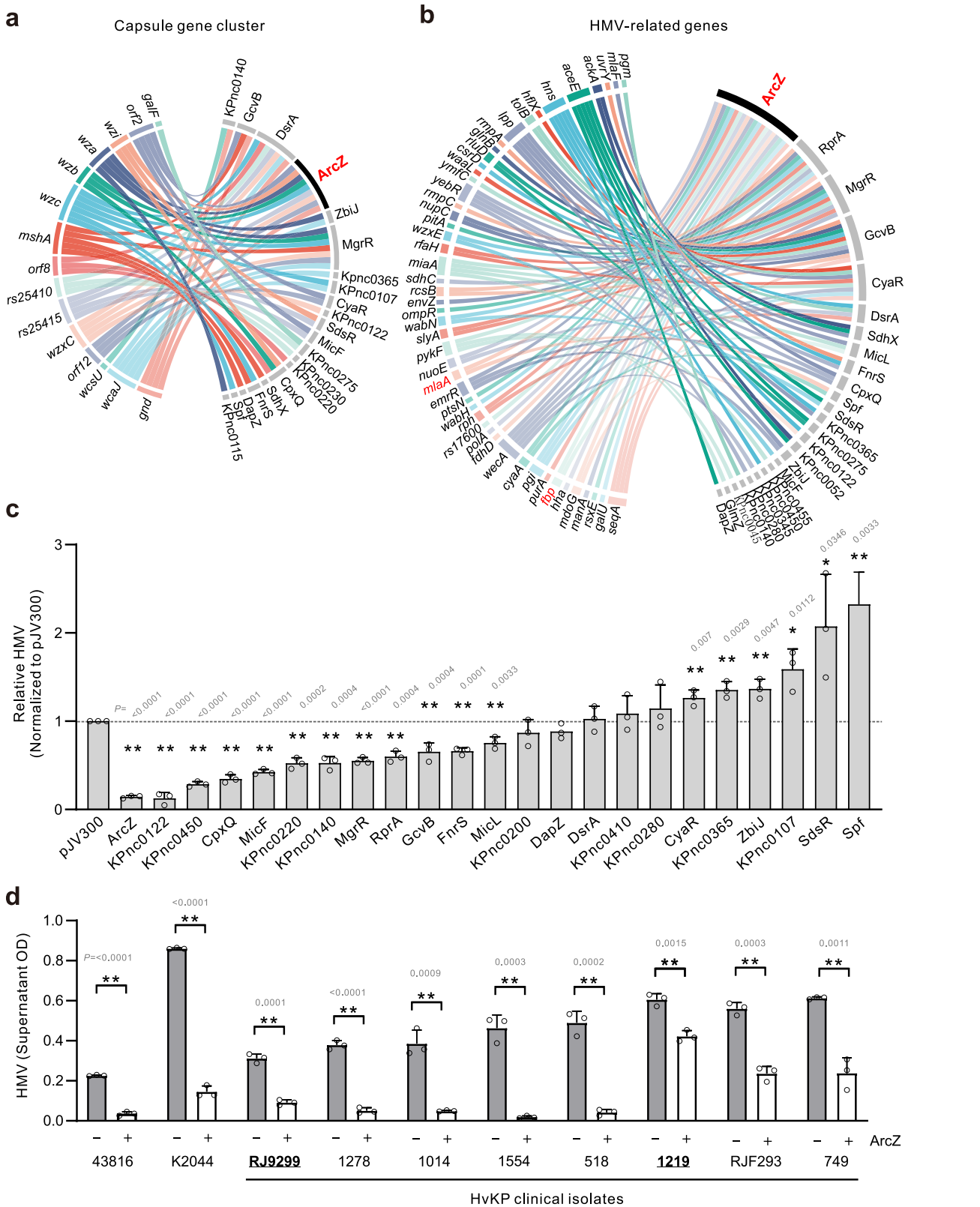

Fig. 2 | The regulatory network of hypermucoviscosity includes many sRNAs. The sRNA-mRNA interaction network involving genes in the capsule biosynthesis cluster (**a**) and known hypermucoviscosity-regulating genes outside the capsule cluster (**b**). See also Supplementary Fig. 7b and Supplementary Data 6. **c** The impact of sRNA overexpression on hypermucoviscosity. Strains containing sRNA expression plasmids were grown overnight in LB containing 1 mM IPTG. Cultures were centrifuged at 1000 *g* for 5 min, and OD_{600} of supernatant was measured and normalized to the OD_{600} of the culture before centrifugation. Relative HMV values are shown relative to the basal HMV level of WT containing a pJV300 control vector. $N = 3$ biological replicates, bars indicate mean ± SD. *, $p < 0.05$; **, $p < 0.01$; two-tailed Student's *t* test. **d** The ArcZ sRNA reduces HMV in different model and clinical strains. Shown in bold and underlined are two clinical CR-HvKP isolates RJ9299 and 1219 (Supplementary Data 7). $N = 3$ biological replicates, bars indicate mean ± SD. *, $p < 0.05$; **, $p < 0.01$; two-tailed Student's *t* test.

observed when the ArcZ-M5 mutant was overexpressed, supporting that ArcZ is a potent and specific inhibitor of HvKP pathogenesis.

The reduced virulence may be due to the diminished expression of ArcZ target genes. Our initial competition experiments revealed that Δ*mlaA* has reduced fitness in mice. The *mlaA* mutant was significantly outcompeted in lungs, whereas it did not show any fitness defect in LB in vitro (Supplementary Fig. 11b). When infecting mice with either WT or Δ*mlaA* in separation, we confirmed that Δ*mlaA* is severely attenuated (Fig. 5g–i), generating ~1000-fold fewer CFU recovered from lung, spleen, and liver 48 h p.i. compared to WT ($p < 0.01$, non-parametric Mann-Whitney U test). Next, we complemented the Δ*mlaA* mutant by introducing a single copy of *mlaA* gene back to the chromosome at another locus. This complementation strain not only restored the expression of MlaA protein (Fig. 5e), and also successfully

Fig. 3 | The ArcZ sRNA is a conserved regulator of multiple HMV-related genes. **a** Genomic context of the *arcZ* gene in *K. pneumoniae*. **b** Multiple sequence alignment of ArcZ sRNA. KPN *K. pneumoniae*, ECO *E. coli*, STM *S.* Typhimurium, CRO *Citrobacter rodentium*, ENT *Enterobacter* spp., SMA *Serratia marcescens*, YPE *Yersinia pestis*, PLU *Photorhabdus luminescens*. The scissors indicate RNase E cleavage site and start of mature ArcZ. **c** HMV is regulated by Δ*arcZ* and a chromosomal complementation of ArcZ. A copy of *arcZ* gene with its own promoter was inserted into *putA* locus by homologous recombination. The i-*wza* mutant serves as negative control. $N = 3$ biological replicates, bars indicate mean ± SD. **: $p < 0.01$; two-tailed Student's *t*-test. **d** ArcZ inhibits the production of capsular polysaccharides. The i-*wza* mutant serves as the acapsular control sample. $N = 3$ biological replicates, bars indicate mean ± SD. *: $p < 0.05$, **: $p < 0.01$; two-tailed Student's *t*-test. **e** Circos plot highlighting the ArcZ interactome. Interactions involving known capsule and HMV-related genes are highlighted in dark blue, tested genes in boldface. The number of S-chimeras are shown in brackets. **f** Regulation of putative target genes by ArcZ. Fluorescence was determined in cells containing translational sfGFP reporters. $N = 3$ biological replicates, bars indicate mean ± SD. *: $p < 0.05$, **: $p < 0.01$, ns: not-significant; two-tailed Student's *t* test. **g**, **h** HMV assay for the *mlaA* and *fbp* mutants. The acapsular i-*wza* mutant served as non-mucoid control. $N = 3$ biological replicates, bars indicate mean ± SD. *: $p < 0.05$, **: $p < 0.01$; two-tailed Student's *t*-test. **i**, **j** Western blot analysis of MlaA and Fbp protein levels, respectively. GroEL served as loading control. The images are representative of three independent experiments. Uncropped blots in Source Data. **k**, **l** Western blot analysis of MlaA and Fbp proteins upon ArcZ overexpression. Cultures were supplemented with 1 mM IPTG to induce ArcZ overexpression. ArcZ containing 2 nt (M2) or 5 nt (M5) mutations (**a**) were included. The images are representative of three independent experiments. Uncropped blots in Source Data.

rescued HMV and pathogenesis similar to the WT levels (Fig. 5f–i). Collectively, these data show that the ArcZ sRNA and its target *mlaA* are crucial regulators of HMV and *Klebsiella* virulence in mice.

MlaA, together with the MlaBCDEF proteins, constitute a phospholipid retrograde transport machinery that maintains lipid asymmetry of the outer-membrane[47,53,54]. MlaA removes misplaced phospholipids in the outer leaflet of outer-membrane, and transports them back to the inner membrane via periplasmic MlaC and the MlaBDEF membrane channel. To better understand the mechanism how MlaA contributes to HMV, we constructed a series of MlaA variants based on the recently solved Cryo-EM structures[47,55,56], generating a number of single-copy chromosomal *mlaA* mutant strains (Fig. 5j). Subsequent analysis revealed that the HMV regulation by MlaA is dependent on several active sites, including residues E163/D166/D169 that are required for phospholipid binding[47], and residues I212-R222 required for interaction with MlaC[56]. These data indicate that phospholipid retrograde transportation is required for HMV, rather than some unknown activity of the MlaA protein in *Klebsiella*. The MlaA* mutant, which induces a "short-circuit" of phospholipid flux in the outer-membrane[47,54], also led to reduced HMV levels, indicating the homeostasis of phospholipid is crucial for HMV. Altogether, our genetic characterizations suggest a molecular model in which MlaA removes free phospholipids in the outer leaflet of outer membrane, provides sufficient space to permit the retention of capsular polysaccharide chains to the cell surface, thus promoting the HMV phenotype.

Transcriptional activation of ArcZ by CRP

To better understand the regulatory circuit of ArcZ, we sought to investigate how the sRNA is activated in *K. pneumoniae*. Previous studies in *E. coli* and *Salmonella* have shown that ArcZ is repressed by the ArcAB two-component system under low-oxygen conditions[42,57], but it is unknown which upstream signals activate ArcZ expression in *K. pneumoniae*. Interestingly, multiple sequence alignment of the ArcZ promoter region from *K. pneumoniae* and other enterobacteria revealed a conserved binding site potentially recognized by CRP, the master regulator of catabolite repression (Fig. 6a). In line with this observation, induction of catabolite repression by glucose suppressed ArcZ expression levels, suggesting that CRP activates ArcZ transcription (Supplementary Fig. 12). We next constructed a Δ*crp* mutant and observed a strong reduction in ArcZ levels. This reduction in Δ*crp* was fully restored to WT levels by the *crp* gene provided in trans (Fig. 6b). Furthermore, the *arcZ* gene with its own promoter (pZE12-P_{own}-*arcZ*) drove higher levels of Pre-ArcZ only in strains with *crp* but not in the Δ*crp* mutant (Fig. 6c). Truncating the potential CRP-binding region from −41 bp upstream (trunc, Fig. 6a; without disturbing the −35 and −10 boxes), or mutating the conserved TCACA motif, both reduced the levels of Pre-ArcZ (Fig. 6c). Although a molecular interaction remains to be proven, these results strongly argue that CRP directly activates the ArcZ promoter. CRP itself acts to repress HMV in *K. pneumoniae*. Deletion of *crp* significantly enhanced the mucoid phenotype, which was fully complemented by the *crp* gene in trans (Fig. 6d). Therefore, we have identified a novel regulatory circuit of HMV, in which the master regulator of catabolite repression CRP activates the ArcZ sRNA, both acting to suppress HMV at the transcriptional and post-transcription level, respectively (Supplementary Fig. 13, Fig. 7).

Discussion

Post-transcriptional control at the RNA level is crucial for bacterial pathogens to coordinate virulence and fitness under changing conditions during host infection. In this study, we generated a comprehensive RNA-RNA interactome map in the hypervirulent pathotype of *K. pneumoniae*, revealing the post-transcriptional regulatory network of virulence control in a superbug of global concern. We discovered that HMV in HvKP is regulated by the major RNA chaperone Hfq and a large number of Hfq-associated sRNAs. Our study further demonstrated the molecular mechanism how ArcZ, as an Hfq-dependent sRNA, regulates HMV and virulence via direct sRNA-mRNA interactions (Fig. 7), adding support to the evolving theory that HMV is critically regulated in *K. pneumoniae* during the process of host infection[58–60]. Our successful identification of key HMV regulators and regulatory circuit in this study may illustrate a new paradigm of using RNA-RNA interactome to guide functional RNA screens with mechanistic precision to understand important traits in different organisms.

Our systems-wide profiling of the RNA interactome in *K. pneumoniae* was achieved by using the iRIL-seq approach, which was recently developed and established in *Salmonella* in our lab[34]. Taking advantage of expressing T4 RNA ligase in vivo[39] and Hfq-coIP[61], iRIL-seq enables proximity-ligation between interacting RNAs in live bacteria and enriches the ligated RNA fragments bound to Hfq. This in vivo approach is highly streamlined compared to crosslinking-dependent RIL-seq[62,63] and CLASH[32], facilitating rapid RNA-interactome analyses in various bacteria and eliminating laborious in vitro ligation and digestion steps[64]. iRIL-seq has been proven to effectively capture sRNA-target interactions at the genome-wide scale in *Salmonella* with high accuracy[34]. Here the RNA-interactome data obtained in HvKP further support the utility of iRIL-seq. Consensus sequence motifs complementary to sRNAs were identified in over 90% of target mRNA genes (Supplementary Fig. 3). Given its simple setup and streamlined workflow, our HvKP dataset further showcases iRIL-seq is a powerful generic approach that can be easily applied to many different organisms to chart functional RNA regulatory networks.

Our study has discovered a large RNA regulatory network involving many HMV-related genes in the HvKP RNA interactome, while numerous known sRNA-mRNA and sRNA-sRNA interactions from *E. coli* and *Salmonella* were also recapitulated. The sRNA regulators of HMV include many core-genome encoded sRNAs conserved in enterobacteria exemplified by ArcZ, and also new sRNA candidates in *Klebsiella* (Fig. 2c, Supplementary Data 2). Several core sRNA regulators have been previously characterized in model organisms. CpxQ

https://doi.org/10.1038/s41467-024-51213-z

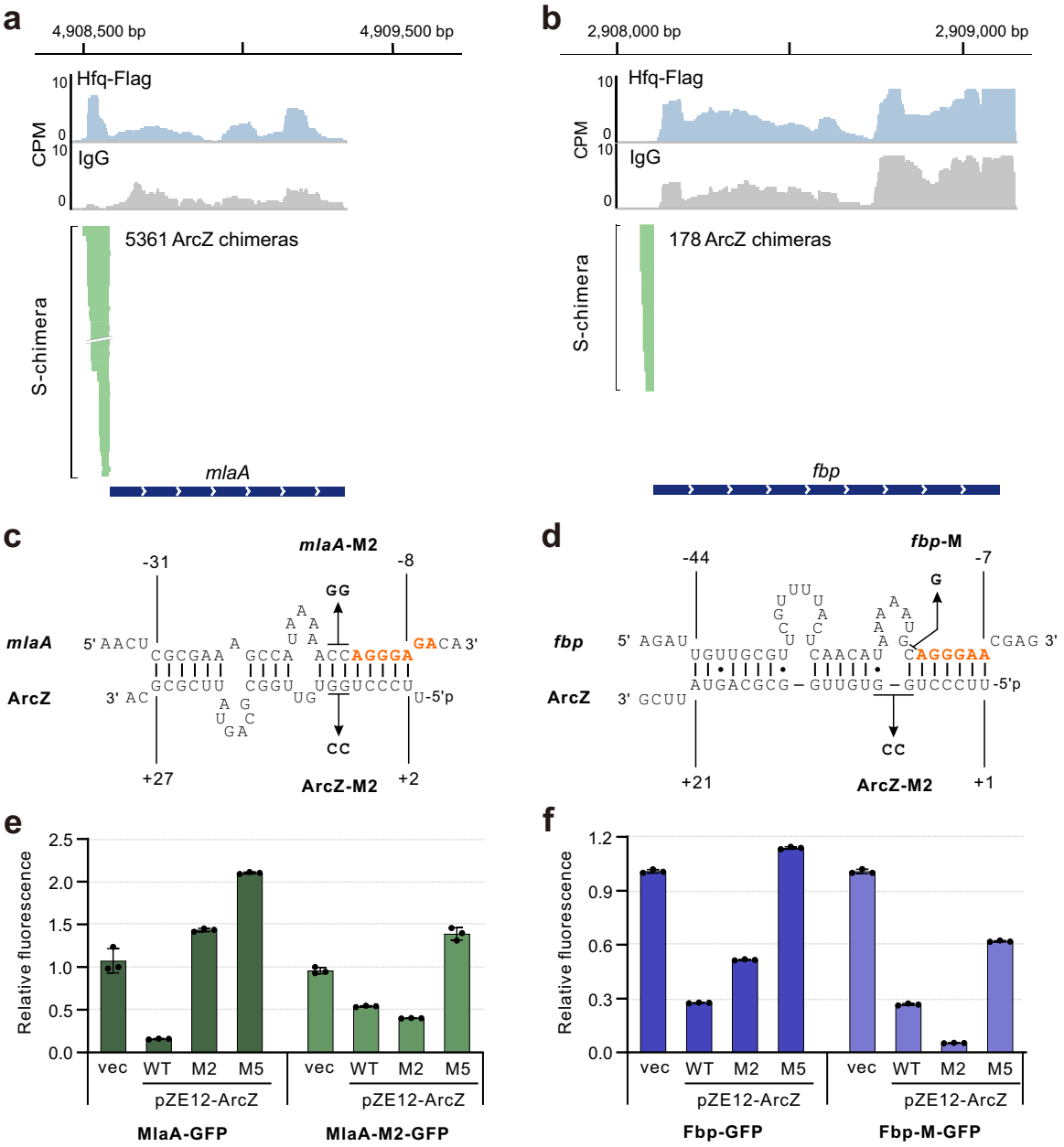

Fig. 4 | ArcZ represses *mlaA* and *fbp* via direct basepairing. Browser images showing the stacked chimeric ArcZ reads mapped in the *mlaA* (**a**) or *fbp* (**b**) loci. The y-axis shows the normalized reads (CPM: counts per million); S-chimera track: Fragments of *mlaA* or *fbp* mRNAs detected in ArcZ S-chimeras in Hfq libraries. Predicted base pairing for ArcZ with *mlaA* (**c**) and *fbp* (**d**). Shine-Dalgarno sequences are shown in red. Numbers indicate the position relative to the start codon of mRNA and numbers below indicate the position in ArcZ. The introduced mutations are indicated. Compensatory basepair exchange analysis to confirm direct interactions with *mlaA* (**e**) and *fbp* (**f**). Fluorescence levels were analyzed for strains expressing MlaA-GFP and Fbp-GFP reporters. $N = 3$ biological replicates, bars indicate mean ± SD.

and MicF function in the envelope stress pathway to target membrane proteins[43,65]; MgrR in the PhoPQ pathway regulates LPS modification and magnesium transport[66,67]; and RprA is an activator of RpoS involved in general stress responses[68]. These sRNAs with diverse functions all strongly inhibit HMV in *K. pneumoniae*, suggesting that sRNAs from several distinct pathways might converge to modulate *Klebsiella* virulence during infection. In a recent study, overexpression of the OmrB sRNA was shown to reduce HMV in another HvKP strain[63]. Besides these core sRNAs, *Klebsiella* sRNA candidates such as KPnc0122, KPnc0450, and KPnc0107 also repressed HMV, providing future opportunities for molecular and functional characterizations.

Our study discovered that the enterobacterial core sRNA ArcZ is integrated into a new regulatory circuit and is endowed with a new function in HvKP (Fig. 7). In *E. coli* and *Salmonella*, the promoter of ArcZ has been shown to be repressed by the ArcAB two-component system[42,57]. Our results suggest that ArcZ, instead of being repressed by ArcAB (Supplementary Fig. 12b), is activated by the catabolite repression protein CRP. This indicates that ArcZ might have evolved with new regulatory functions under the control of CRP. Functional enrichment analysis for the ArcZ targets revealed several significant pathways related to carbohydrate and polysaccharide metabolism (Supplementary Fig. 7a), consistent with the observed repressive roles on HMV (Fig. 2c, d) and capsule production (Fig. 3d, Supplementary Fig. 4c). Total RNA-seq analysis also revealed significant down-regulation of capsule genes upon ArcZ overexpression (Supplementary Fig. 8), although direct base-pairings remain to be verified. Our results suggest

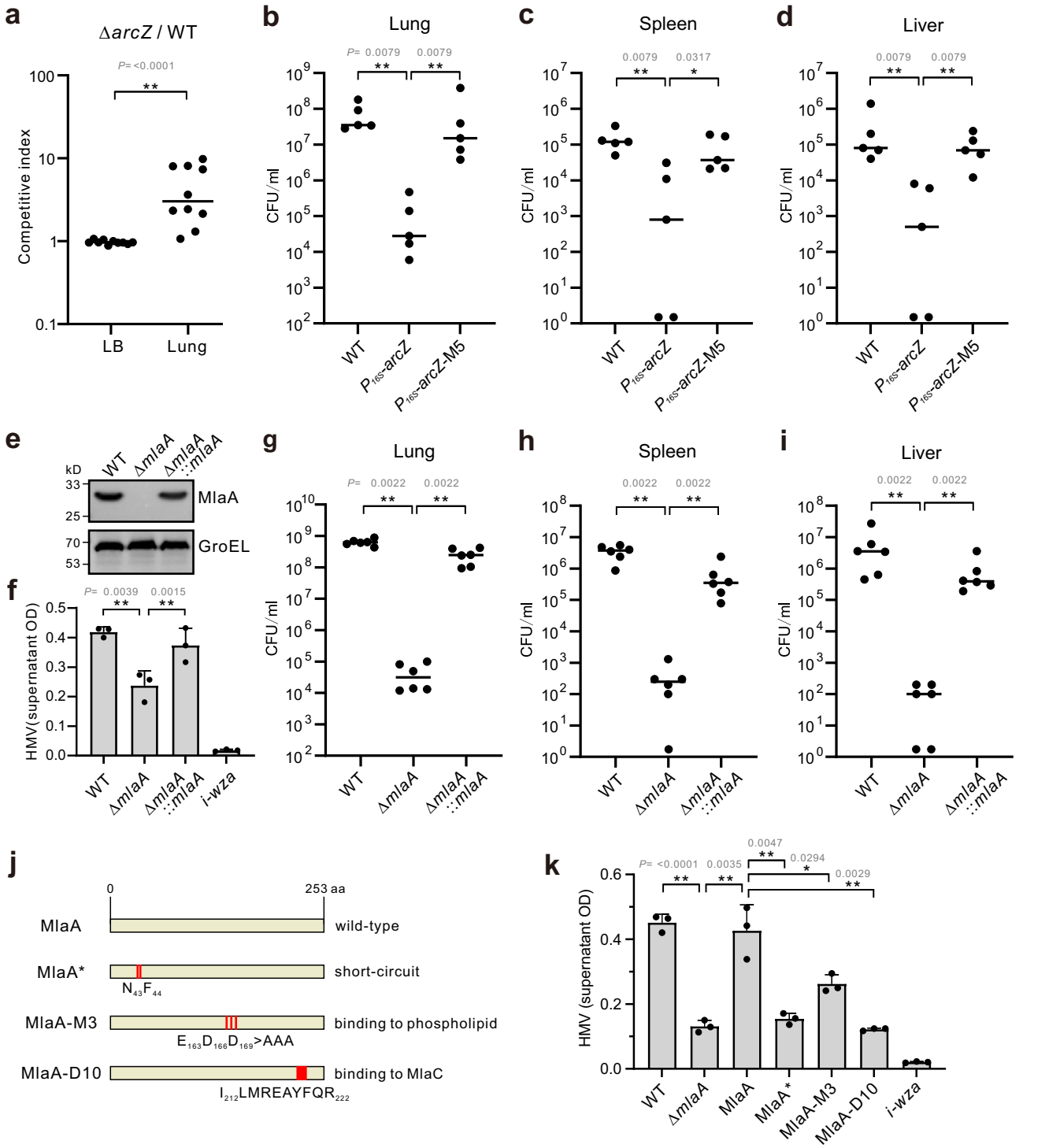

that even conserved sRNAs may have evolved distinct functions in different organisms. Likewise, a recent study showed that the homologs of ArcZ in *Photorhabdus*/*Xenorhabdus* regulate metabolite production and symbiosis with nematodes[46,69].

CRP controls one of the largest regulons to modulate bacterial carbon metabolism and energy expenditure. Consistent with previous reports[20,70], our study suggests that CRP is a negative regulator of HMV. CRP was shown to repress the transcription of capsule gene clusters via direct binding to the promoters. In the meantime, CRP activates the ArcZ sRNA, which in turn binds and represses many other HMV-related mRNAs. ArcZ may function as an extension of CRP to repress more HMV genes at the post-transcriptional level (Fig. 7). We note that the CRP pathway may be more complicated than this simple model. Besides ArcZ, CRP regulates two other sRNAs, Spf and CyaR, according to studies in *E. coli* and *Salmonella*[71,72]. Both sRNAs positively regulated HMV, in contrast to the repressive roles of ArcZ and Hfq. Thus, sRNAs within the CRP pathway both negatively and positively regulate HMV, indicating the existence of complicated regulatory loops fine-tuning HMV at the post-transcriptional level[73].

We show for the first time that the phospholipid trafficking pathway is crucial for *Klebsiella* virulence and that MlaA is an essential virulence factor in HvKP (Fig. 5g–i). As a key target of ArcZ, *mlaA* encodes the crucial outer membrane component of the Mla phospholipid retrograde transportation system that maintains lipid

https://doi.org/10.1038/s41467-024-51213-z

Fig. 5 | ArcZ and MlaA are crucial for *Klebsiella* virulence in mouse. **a** Competition assay using a 1:1 mixture of WT and Δ*arcZ* mutant. Mice were inoculated with 10^3 CFU of the mixed bacteria intranasally, and scarified 48 h pi for enumeration. Growth competition in LB serves as in vitro control. $N = 10$ biological replicates, lines indicate median value. **, $p < 0.01$; two-tailed Mann-Whitney U test. ArcZ overexpression significantly reduced *Klebsiella* pathogenesis in mice. Bacterial burden in lung (**b**), spleen (**c**), and liver (**d**) were enumerated 48 h pi. Samples below limit of detection (100 CFU) are drawn on X-axis. $N = 5$ biological replicates, lines indicate median value. *, $p < 0.05$; **, $p < 0.01$; two-tailed Mann-Whitney U test. One-way ANOVA test with post-hoc Tukey's multiple comparisons: $p < 0.05$ (**c**). **e** Western blot verification of MlaA expression in the chromosomal deletion and complementation strains. 3xFLAG tag was introduced into the C-terminus of MlaA and used for detection by anti-FLAG antibody. GroEL serves as loading control. Experiment was performed three times. Uncropped blots in Source Data. **f** MlaA is required for HMV. The HMV level was determined with overnight cultures of indicated strains. Chromosomal complementation was constructed by inserting a copy of *mlaA* gene with its own promoter into *putA* locus using homologous recombination. The acapsular i-*wza* mutant served as negative control. $N = 3$ biological replicates, bars indicate mean ± SD. *, $p < 0.05$; **, $p < 0.01$; two-tailed Student's *t*-test. **g**–**i** MlaA is required for *Klebsiella* pathogenesis. Mice were infected with 10^3 CFU of indicated strains via intranasal instillation. Bacterial burdens were analyzed 48 h pi. $N = 6$ biological replicates, lines indicate median value. **, $p < 0.01$, two-tailed Mann-Whitney U test. One-way ANOVA test with post-hoc Tukey's multiple comparisons: $p < 0.001$ (**g**, **h**). **j** Mutations introduced in the MlaA protein variants and their associated molecular functions. **k** HMV analysis for strains with chromosomal MlaA variants. The *mlaA* gene containing desired mutations was introduced back into the chromosome of Δ*mlaA* strain. $N = 3$ biological replicates, bars indicate mean ± SD. *, $p < 0.05$; **, $p < 0.01$; two-tailed Student's *t*-test.

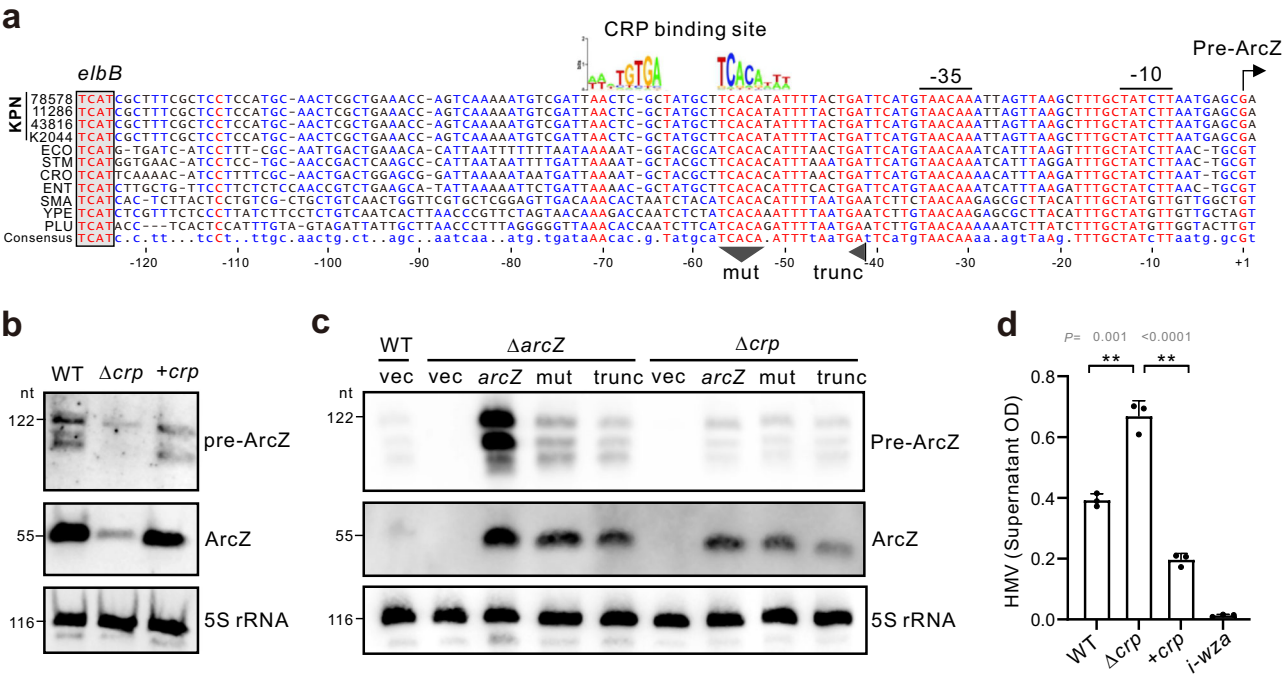

Fig. 6 | CRP activates the transcription of ArcZ in *K. pneumoniae*. **a** Multiple sequence alignment of the ArcZ promoter region. The putative CRP-binding site is labeled. **b** Expression of ArcZ requires the transcriptional regulator CRP. Northern blot was performed using 10 mg total RNA extracted from the indicated strains. Pre-ArcZ was detected using probe YCO-1838, the mature ArcZ was detected using probe YCO-1745. 5S rRNA served as loading control. Experiment was performed three times. Uncropped blots in Source Data. **c** Northern blot analysis to identify critical region in *arcZ* promoter. ArcZ expression from pZE12-based plasmids carrying different *arcZ* genomic regions. Vec, empty vector control (pJV300); *arcZ*, plasmid carrying an *arcZ* gene with native promoter; Mut: mutation of the conserved TCACA sequence. Trunc: truncation of the ArcZ promoter from −41 bp upwards without disturbing the *arcZ* gene. 5S rRNA was probed as loading control. Experiment was performed three times. Uncropped blots in Source Data. **d** CRP negatively regulates HMV. Overnight cultures of the indicated strains were centrifuged at 1000 *g* for 5 min. $N = 3$ biological replicates, bars indicate mean ± SD. *, $p < 0.05$; **, $p < 0.01$; two-tailed Student's *t*-test.

asymmetry and membrane integrity[47,48,53]. Deletion of *mlaA*, without showing any growth or fitness defect in LB broth (Supplementary Fig. 11b), resulted in a strong reduction of HMV and a severe attenuation of virulence in the murine model of infection (Fig. 5). Transposon disruption of *mlaBCDEF* genes also led to decreased HMV[19], supporting the involvement of the entire Mla system and its molecular function. Our further mutational analysis of MlaA revealed that phospholipid transport activity is crucial for capsule retention and HMV, providing a new mechanism underlying the HMV phenotype. Because the Δ*mlaA* mutant still retains a low level of HMV higher than the acapsular control (Fig. 5f), its strong attenuation in virulence makes Δ*mlaA* an attractive candidate to develop live attenuated vaccine. MlaA might also represent an interesting drug target located on the bacterial surface for the future development of therapeutics against HvKP. On the same note, ArcZ may also be exploited as a potential anti-infection drug in the form of antisense RNA therapeutics[74,75]. Our data demonstrated that ArcZ is effective to reduce HMV in a variety of clinical HvKP strains including CR-HvKP isolates, which urgently demand new treatment options in clinics.

Methods

All the experiments comply with the ethical regulations at the Shanghai Institute of Immunity and Infection, Chinese Academy of Sciences. The animal experiments were conducted following institutional ethics requirements under the animal facility user permit (No. IPS-26-CYJ), and the infection experiments were performed following the animal protocol (A2022053) approved by the institutional animal care and ethics committee. The collection of clinical isolates was approved by the medical science research ethic committee of Peking University Third Hospital (M3022382).

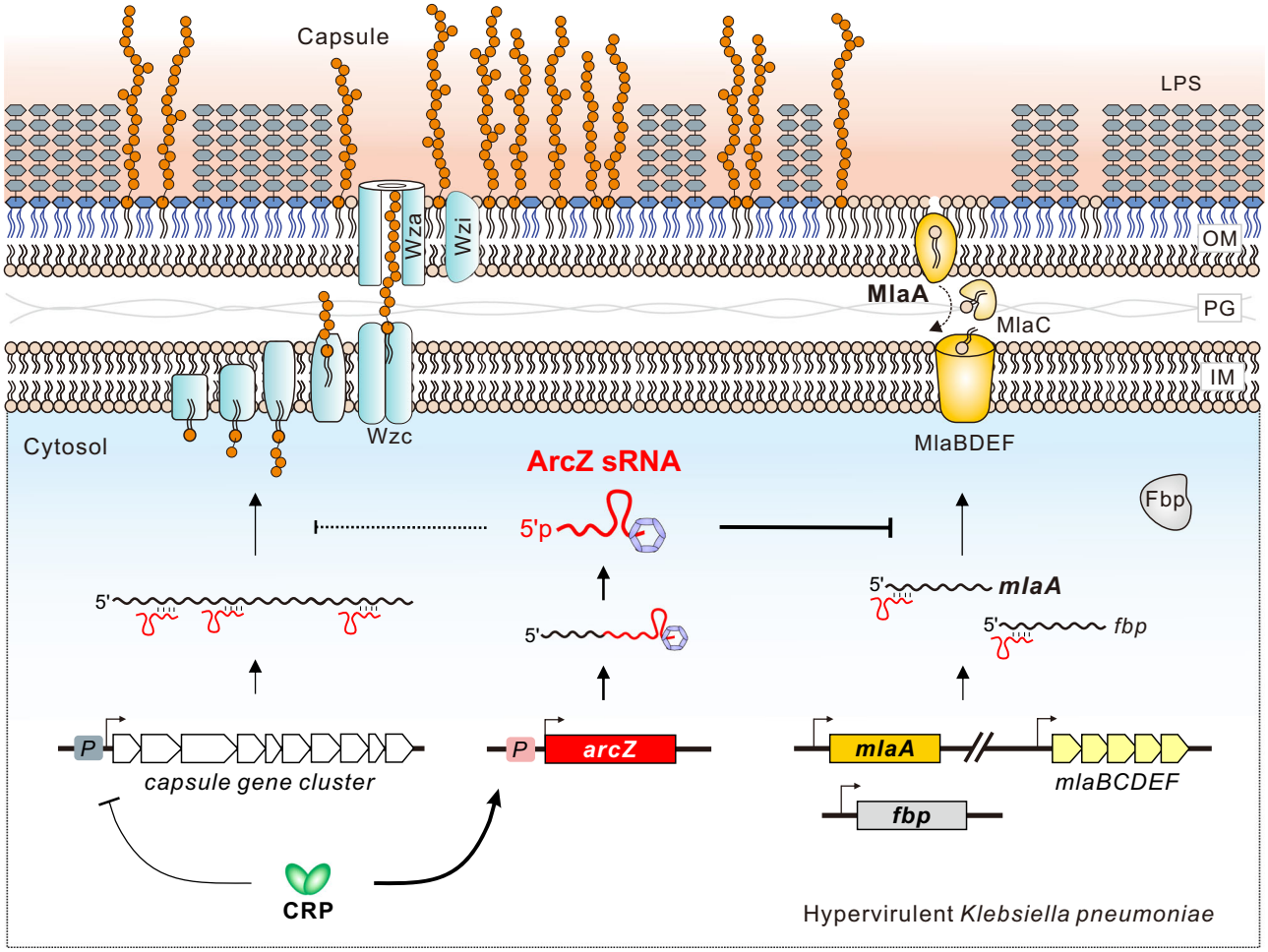

Fig. 7 | Regulatory circuit of ArcZ-mediated HMV regulation in *K. pneumoniae*. Mucoid capsular polysaccharides are synthesized and translocated across membrane relying on protein products translated from the capsule gene cluster (e.g., Wza, Wzc, Wzi). The transcription of capsule genes is repressed by CRP via direct binding to the promoters; whereas their translation may be repressed by ArcZ at the RNA level. CRP activates the transcription of ArcZ precursor, which is further processed into a shorter mature ArcZ sRNA. Via direct RNA base-pairing interactions, ArcZ binds to the HMV-related mRNAs such as *mlaA* and *fbp* and inhibit their translation initiation. Reduced MlaA synthesis disrupts OM lipid asymmetry and homeostasis of phospholipid retrograde transport from outer leaflet, thereby interfering with the retention of capsular polysaccharides on the OM and proper level of HMV, abrogating *Klebsiella* virulence in mice. OM outer-membrane, IM inner-membrane, PG peptidoglycan, LPS Lipopolysaccharides.

Bacterial strains and growth conditions

Hypervirulent *Klebsiella pneumoniae* ATCC 43816 is used as wild-type. Information on the clinical isolates is available in *Supplementary Methods* and Supplementary Data 7. Mutant strains generated in this study are described in Supplementary Data 8. Unless otherwise stated, bacteria were grown in LB medium (10 g/L tryptone, 5 g/L yeast extract, and 5 g/L NaCl) with 220 rpm aeration or on LB agar at 37 °C. Where appropriate, antibiotics were used at the following concentrations: 20 μg/ml chloramphenicol, 50 μg/ml kanamycin, 50 μg/ml spectinomycin, 100 μg/ml hygromycin B, and 50 μg/ml apramycin sulfate. 1 mM IPTG was used for the induction of sRNA expression from pZE12 plasmids.

Deletion strains and chromosomally 3xFLAG epitope tag strains were constructed using the λ Red system[76,77]. To construct the Δ*arcZ* mutant, wild-type *Klebsiella* cells carrying the temperature-sensitive pACBSR-Hyg helper plasmid were transformed with 1 μg dsDNA fragments, which were amplified using YCO-1438/-YCO-1439 and pFLP-hyg as template. Desired recombinants were confirmed by resistance to apramycin, and by colony PCR with YCO-1038/-YCO-1039 and Sanger sequencing. To introduce 3xFLAG epitope tags, DNA fragments were amplified by PCR with primer pairs YCO-1447/1448 and pSUB11 as template, and electroporated into competent cells expressing λ Red recombinase from pACBSR-Hyg. Correct transformants were selected on kanamycin plates and confirmed by colony PCR.

Chromosomally complemented strains were constructed using the λ Red system and from pACBSR-Hyg[76,77]. DNA fragments were amplified from pXG10 vectors containing resistance maker and P_{own}-*arcZ* or P_{own}-*mlaA* fragments by primer pairs YCO-2321/2322, and electroporated into mutant strains lacking either *arcZ* or *mlaA*. Point mutations in MlaA were first introduced into the pXG10-P_{own}-*mlaA* vector by site-directed mutagenesis using primers described in Supplementary Data 8. Mutated *mlaA* fragments were amplified using oligos YCO-2321/2322, and electroporated into Δ*mlaA* competent cells expressing λ Red recombinase. The DNA fragments were inserted into the *putA* locus on chromosome by homologous recombination as previously described[78]. Correct transformants were selected on chloramphenicol plates, and confirmed by colony PCR and Sanger sequencing.

Plasmids construction

The oligonucleotides and plasmids used in this study are listed in Supplementary Data 9 and 10, respectively. To express a plasmid-borne *t4rnl1* gene from the tightly controlled, L-arabinose-inducible pBAD promoter, pBAD-Hyg was amplified by PCR with oligonucleotides

YCO-0453/−0454, and the *t4rnl1* gene was amplified from pKH13-*t4rnl1* using oligonucleotides YCO-0905/−0906. Vector and insert were ligated following restriction digestion with *Xba*I. Overexpression plasmids for sRNAs were constructed using pZE12-luc as the scaffold plasmid[43]. Here, an *Xba*I-digested PCR product obtained by amplification of pZE12-luc with primers YCO-0557/−0558 was ligated to sRNAs amplified from genomic DNA, and similarly digested with *Xba*I. Construction of GFP translational fusion plasmids were carried out principally as described[43], using the pXG10-SF or pXG30-SF. The pXG10-SF vector was used for monocistronic genes, the pXG30 vector for operons. Briefly, the pXG10-SF backbone was amplified with YCO-1437/−1398, and pXG30-SF backbone was amplified with YCO-1806/−1398 or YCO-1940/−1398. The 5′ regions of target genes, including regions captured in the chimeric fragments, were PCR amplified, digested with *Nsi*I/*Pst*I and *Nhe*I, and cloned into pXG10-SF or pXG30-SF backbones digested with the same restriction enzymes. All the plasmids and insertions were verified by colony PCR and Sanger sequencing.

HMV quantification

K. pneumoniae strains were grown overnight in 3 ml LB medium at 37 °C. Next, 1 ml of culture was centrifuged for 5 min at 1000 × *g* (room temperature), and the OD_{600} of the upper 200 µl supernatant was determined. Final readings were normalized to the OD_{600} in the input culture before centrifugation. At least three biological replicates were prepared for each strain.

Capsule purification and quantification

K. pneumoniae was grown overnight in 1 mL LB medium with 220 rpm at 37 °C. Cultures were added with 100 µl the capsule extraction buffer (500 mM citric acid pH 2.0, 1% Zwittergent 3-10), incubated at 50 °C for 20 min. Cells were pelleted, and the supernatant was mixed with an equal volume of isopropanol, followed by precipitation for 30 min at 4 °C. The capsule was centrifuged for 10 min at maximum speed and resuspended in 150 µl PBS. Protein and membrane contaminants were removed by adding 100 µl buffer P2 (TIANGEN) and 125 µl buffer P3 (TIANGEN). The clarified supernatant was precipitated with an equal volume of isopropanol for 30 min at 4 °C. The capsule was centrifuged at maximum speed for 30 min at 4 °C and washed twice with 75% ethanol. The purified capsule was resuspended in nuclease-free water and confirmed on SDS-PAGE by alcian blue staining. The uronic acid assay was used to quantify the amounts of capsular polysaccharides. 12.5 mM borax (Sangon) in H_2SO_4 was added to samples and boiled before chilling on ice. Followed by addition of 0.15% 3-hydroxydiphenol (Sigma-Aldrich), the mixture was analyzed by the absorbance at 520 nm. Uronic acid content was determined from a standard curve of glucuronic acid (Sangon) and normalized as micrograms per 1 OD of bacterial culture.

Hfq-coIP experiments

The Hfq-coIP was performed using our previously published protocol[61]. *K. pneumoniae hfq*::3xFLAG strain containing the plasmid pYC582 was grown in LB medium with 220 rpm at 37 °C. T4 RNA ligase 1 was induced for 30 min by adding 0.2% L-arabinose when the culture reached OD_{600} of 3.0. Bacterial samples (~100 OD) were collected by centrifugation at 4000 *g* for 20 min at 4 °C. The bacterial pellets were resuspended in 500 µl ice-cold lysis buffer (20 mM Tris pH 8.0, 150 mM KCl, 1 mM of $MgCl_2$, 1 mM DTT, 0.05% Tween-20), and broke with 500 µl glass beads using the Cryolys Evolution instrument for 15 min at 4 °C. Lysates were collected by centrifugation at 16,000 *g* for 30 min at 4 °C, and divided into new tubes equally. Cleared lysates were respectively incubated with anti-FLAG antibody (Sigma) or IgG isolate control (Invitrogen) conjugated on the protein-G magnetic beads (Thermo-Fisher) for 1 h at 4 °C with rotation. The beads were collected by the magnet, and washed five times with 500 µl lysis buffer and resuspended in 50 µl lysis buffer. The Hfq-bound RNA was extracted by RNA clean & concentrator columns (Sangon, Shanghai). The purified RNA was resuspended in nuclease-free water.

RNA extraction

Total RNA was extracted using TRIzol reagent. Briefly, 4 OD of cells were collected with addition of 0.2 vol/vol of STOP solution (95% ethanol, 5% phenol), centrifuged for 5 min, 16,000 *g* at 4 °C and the supernatant was discarded. For cell lysis, pellets were resuspended with 500 µl lysozyme (A610308, BBI) at 0.5 mg/ml. Cleared lysates were mixed with 1 ml TRIzol and incubated for 10 min at room temperature with shaking. Subsequently, 400 µl chloroform was added, mixed by inversion, and incubated for 5 min at room temperature to allow phase separation. After the samples were centrifuged for 15 min, 16,000 *g* at 4 °C, the upper phase was transferred to a new tube and 700 µl isopropanol was added and incubated overnight at −20 °C. Finally, samples were centrifuged, washed with cold 75% v/v ethanol and air-dried for 15 min. Precipitated RNA was resuspended in 30 µl nuclease-free water and stored at −80 °C.

Northern blotting

Ten micrograms of total RNA were denatured at 98 °C for 2 min in RNA loading buffer (98% formamide, 1 mM EDTA, 0.1% xylene cyanol, 0.1% Bromphenol blue) and separated on 7 M urea/6% polyacrylamide gels in 1 × TBE buffer. RNAs were transferred onto Hybond-N+ membranes (GE Healthcare) by electroblotting (50 V) for 1 h at 4 °C and fixed to the membrane by UV crosslinking (120 mJ). Detection was performed using the Roche DIG system. Each primary probe was designed to contain an overhang sequence that is complementary the digoxigenin-labeled secondary probe YCO-0550. For instance, mature ArcZ was detected using the specific complementary probe YCO-1745, while CyaR was detected using primary probe YCO-1784. Both primary probe-hybridized sRNAs were detected with secondary probe YCO-0550. Membranes were prehybridized in DIG Easy Hyb (#11796895001, Roche) for 30 min. DNA probes were hybridized overnight at 42 °C. Membranes were washed with 5× SSC/0.1% SDS, 1× SSC/0.1% SDS, and 0.5× SSC/0.1% SDS buffers for 15 min each. Following one wash with maleic acid wash buffer (0.1 M maleic acid, 0.15 M NaCl, 0.3% V/V Tween-20, pH 7.5) for 15 min at 37 °C and blocked with blocking solution (#11096176001, Roche) for 1 h at 37 °C, membrane was hybridized with 75 mU/ml Anti-Digoxigenin-AP (#11093274910, Roche) in blocking solution for 60 min at 37 °C. Wash membrane twice (2 × 15 min) with maleic acid wash buffer and equilibrate membrane 3 min in Detection Buffer (0.1 M Tris−HCl, 0.1 M NaCl, pH 9.5). Signals were visualized by CDP-star (#11759051001, Roche) on a ChemScope imaging station and quantified using ImageJ Software.

Western blotting

Bacterial cells were collected by centrifugation for 5 min at 16,000 g at 4 °C, and pellets were resuspended in protein loading buffer. After heating for 5 min at 95 °C, 0.05 OD_{600} equivalents of samples were separated on 12% SDS-PAGE gel and transferred to PVDF membranes (polyvinylidene fluoride, #10600023, Amersham). Membranes were blocked for 1 h with 5% (w/v) milk powder in TBS-T (Tris-buffered saline-Tween-20) and incubated overnight with primary antibody (monoclonal anti-FLAG, 1:10,000, Sigma #F1804-5MG; anti-GroEL, 1:10,000, Sigma; or anti-GFP, 1:10,000, Roche #11814460001 in 3% bovine serum albumin (BSA)/TBS-T) at 4 °C. Following three washes for 10 min in 1× TBST buffer, membranes were incubated with secondary anti-mouse or anti-rabbit HRP (horseradish peroxidase)-linked antibodies (#D110087-0100 or #D110058-0100, BBI; 1:10000) diluted in 1× TBST buffer containing 1% skim milk. After another three washes for 10 min in 1× TBST buffer, chemiluminescent signals were developed using ECL Prime reagents (#C500044-0100, Sangon) visualized on a ChemScope imaging station and quantified using ImageJ software.

iRIL-seq cDNA library construction

iRIL-seq libraries were constructed using the RNAtag-seq method as described previously[34,64]. Briefly, fragmented RNA was treated with DNase I and FastAP. RNA then was ligated to the 3′ barcoded adapter, and depleting ribosomal RNA by Ribo-off rRNA depletion Kit (#N407-01, Vazyme). First strand cDNA was synthesized by HiScript II 1st Strand cDNA Synthesis Kit (#R211-01, Vazyme), and RNA was degraded after reverse transcription by 1 M NaOH and 0.5 M acetic acid. The cDNA was ligated to a second adapter. Samples were purified with 2.5x Agencourt AMPure XP beads and 1.5x isopropanol. Libraries were amplified by PCR with Illumina P5 and P7 primers using Q5 High-Fidelity DNA Polymerase (#M0491L, NEB), and purified with 1.5x AMPure XP beads. The libraries were sequenced by 150 bp paired-end sequencing with an Illumina NovaSeq instrument.

iRIL-seq data computational analysis

Data analysis was performed using the method reported by Melamed et al. [31,64]. with minor modifications. Briefly, clean reads were generated from raw sequencing reads by removing adapter sequences and low-quality sequences using FASTXToolkit (Version 0.0.13), and reads less than 25 nt were discarded. The first 25 nucleotides of each remaining read were mapped to the genome of *K. pneumoniae* ATCC 43816 (GenBank: NZ_CP009208.1), sorting the fragments into "single" and "chimeric" fragments. Fragments that mapped within a distance of 1000 nt were considered single, whereas fragments that mapped to two different loci were considered chimeric. More details can be found in *Supplementary Methods*.

Total RNA-seq analysis

RNA-seq libraries were constructed by Novogene Group, Beijing, China. The cDNA libraries were sequenced on Illumina NovaSeq X plus. We used cutadapt 2.10 and fastx toolkit 0.0.14 to clip the adapter sequences and quality filtering. Reads unambiguously aligned to unique position in the reference genome (GenBank: NZ_CP009208.1) were preserved to calculate reads number, CPM (counts per million), and RPKM (reads per kilobase and per million) for each gene. Differential expression was tested using DESeq2, generating *p*-value and FDR based on the model of negative binomial generalized linear model.

Fluorescence analysis

Single colonies of *Klebsiella* strains harboring superfolder GFP (sfGFP) translational fusions and sRNA expression plasmids were inoculated into LB medium and grown overnight at 37 °C. The following day, 100 μl of overnight cultures were centrifuged and the pellets were resuspended in 1 ml of PBS. OD_{600} and fluorescence (excitation at 476 nm and emission at 510 nm, using emission cutoff filter of 495 nm) was measured using the Agilent BioTek Synergy H1 plate reader. Fluorescence measurements were normalized to the OD_{600} of cultures. Background fluorescence from control samples not expressing fluorescent proteins was subtracted from experimental samples. The level of regulation was calculated as the ratio between the fluorescence level of a strain carrying the sRNA over-expressing plasmid and a strain carrying the control plasmid. Three biological replicates were prepared for each strain.

Animal infection experiments

Six-to-eight weeks old female Balb/C mice were used and housed at 22 °C with a 12-h light/dark cycle and 45% humidity. Chow and water were provided *ad libitum*. Mice were randomly assigned to experimental groups, with at least five mice per group. Prior to infection, mice were anaesthetized via intraperitoneal injection of tribromoethanol (0.2 ml/10 g). Mice were intranasally infected with ~10^3 CFUs (in 25 μl PBS) per bacterial strain, or a total of 10^3 CFUs in competition assays. Mice were weighted daily until the end of experiment. Approximately 48 h post-infection, mice were euthanized and organs including lung, liver, and spleen were processed for CFU analysis. Serial dilution of CFUs were plated on LB agar plates with appropriate antibiotics and incubated overnight at 37 °C.

Statistical analysis

Experiments were repeated at least three times. At least five mice per group were used for animal infection assays. Mean values and standard deviations were shown in figures. Statistical significance (*P* values) was analyzed using the GraphPad software (version 9) with 95% confidence interval.

Reporting summary

Further information on research design is available in the Nature Portfolio Reporting Summary linked to this article.

Data availability

The sequencing data have been deposited in the GEO database under accession numbers GSE243246 and GSE260738. Raw data, materials, and regents are available upon request. Source data are provided with this paper.

References

1. Wyres, K. L., Lam, M. M. C. & Holt, K. E. Population genomics of Klebsiella pneumoniae. *Nat. Rev. Microbiol.* **18**, 344–359 (2020).
2. Liu, Z. et al. CpxR promotes the carbapenem antibiotic resistance of Klebsiella pneumoniae by directly regulating the expression and the dissemination of blaKPC on the IncFII conjugative plasmid. *Emerg. Microbes Infect.* **12**, 2256427 (2023).
3. Pendleton, J. N., Gorman, S. P. & Gilmore, B. F. Clinical relevance of the ESKAPE pathogens. *Expert Rev. Anti Infect. Ther.* **11**, 297–308 (2013).
4. Rice, L. B. Progress and challenges in implementing the research on ESKAPE pathogens. *Infect. Control Hosp. Epidemiol.* **31**, S7–S10 (2010).
5. Liu, Y.-C., Cheng, D.-L. & Lin, C.-L. Klebsiella pneumoniae liver abscess associated with septic endophthalmitis. *Arch. Intern. Med.* **146**, 1913–1916 (1986).
6. Piednoir, P. et al. Spontaneous community-acquired bacterial meningitis in adults admitted to the intensive care units in the Caribbean French West Indies: unusual prevalence of Klebsiella pneumonia. *Int. J. Infect. Dis.* **100**, 473–475 (2020).
7. Zou, Q. & Li, Y. Hypervirulent Klebsiella pneumoniae. *N. Engl. J. Med.* **385**, 833 (2021).
8. Tian, D. et al. Prevalence of hypervirulent and carbapenem-resistant Klebsiella pneumoniae under divergent evolutionary patterns. *Emerg. Microbes Infect.* **11**, 1936–1949 (2022).
9. Yang, X. et al. Molecular epidemiology of carbapenem-resistant hypervirulent Klebsiella pneumoniae in China. *Emerg. Microbes Infect.* **11**, 841–849 (2022).
10. Zhang, R. et al. Emergence of carbapenem-resistant serotype K1 hypervirulent Klebsiella pneumoniae strains in China. *Antimicrob. Agents Chemother.* **60**, 709–711 (2016).
11. Zhu, J., Jiang, X., Zhao, L. & Li, M. An outbreak of ST859-K19 carbapenem-resistant hypervirulent Klebsiella pneumoniae in a Chinese teaching hospital. *mSystems* **7**, e0129721 (2022).
12. Walker, K. A. & Miller, V. L. The intersection of capsule gene expression, hypermucoviscosity and hypervirulence in Klebsiella pneumoniae. *Curr. Opin. Microbiol.* **54**, 95–102 (2020).
13. Paczosa, M. K. & Mecsas, J. Klebsiella pneumoniae: going on the offense with a strong defense. *Microbiol. Mol. Biol. Rev.* **80**, 629–661 (2016).
14. Cheng, H. Y. et al. RmpA regulation of capsular polysaccharide biosynthesis in Klebsiella pneumoniae CG43. *J. Bacteriol.* **192**, 3144–3158 (2010).
15. Lai, Y.-C., Peng, H.-L. & Chang, H.-Y. RmpA2, an activator of capsule biosynthesis in Klebsiella pneumoniae CG43, regulates K2 cps gene

expression at the transcriptional level. *J. Bacteriol.* **185**, 788–800 (2003).
16. Ovchinnikova, O. G. et al. Hypermucoviscosity regulator RmpD interacts with wzc and controls capsular polysaccharide chain length. *mBio* **14**, e0080023 (2023).
17. Walker, K. A., Treat, L. P., Sepúlveda, V. E. & Miller, V. L. The small protein RmpD drives hypermucoviscosity in Klebsiella pneumoniae. *mBio* **11**, e01750–20 (2020).
18. Walker, K. A. et al. A Klebsiella pneumoniae regulatory mutant has reduced capsule expression but retains hypermucoviscosity. *mBio* **10**, e00089-19 (2019).
19. Dorman, M. J., Feltwell, T., Goulding, D. A., Parkhill, J. & Short, F. L. The capsule regulatory network of Klebsiella pneumoniae defined by density-TraDISort. *mBio* **9**, e01863-18 (2018).
20. Lin, C.-T. et al. Role of the cAMP-dependent carbon catabolite repression in capsular polysaccharide biosynthesis in Klebsiella pneumoniae. *PLoS ONE* **8**, e54430 (2013).
21. Mike, L. A. et al. A systematic analysis of hypermucoviscosity and capsule reveals distinct and overlapping genes that impact Klebsiella pneumoniae fitness. *PLoS Pathog.* **17**, e1009376 (2021).
22. Ou, Q. et al. Involvement of cAMP receptor protein in biofilm formation, fimbria production, capsular polysaccharide biosynthesis and lethality in mouse of Klebsiella pneumoniae serotype K1 causing pyogenic liver abscess. *J. Med. Microbiol.* **66**, 1–7 (2017).
23. Wang, L. et al. Two-component response regulator OmpR regulates mucoviscosity through energy metabolism in Klebsiella pneumoniae. *Microbiol Spectr.* **11**, e0054423 (2023).
24. Chiang, M.-K., Lu, M.-C., Liu, L.-C., Lin, C.-T. & Lai, Y.-C. Impact of Hfq on global gene expression and virulence in Klebsiella pneumoniae. *PLoS ONE* **6**, e22248 (2011).
25. Huang, S.-H. et al. Role of the small RNA RyhB in the Fur regulon in mediating the capsular polysaccharide biosynthesis and iron acquisition systems in Klebsiella pneumoniae. *BMC Microbiol.* **12**, 148 (2012).
26. Hör, J., Matera, G., Vogel, J., Gottesman, S. & Storz, G. Trans-acting small RNAs and their effects on gene expression in Escherichia coli and Salmonella enterica. *EcoSal Plus* **9**, 1–24 (2020).
27. Vogel, J. & Luisi, B. F. Hfq and its constellation of RNA. *Nat. Rev. Microbiol.* **9**, 578–589 (2011).
28. Chao, Y. & Vogel, J. The role of Hfq in bacterial pathogens. *Curr. Opin. Microbiol.* **13**, 24–33 (2010).
29. Papenfort, K. & Melamed, S. Small RNAs, Large Networks: Post-transcriptional regulons in Gram-negative bacteria. *Annu. Rev. Microbiol.* https://doi.org/10.1146/annurev-micro-041320-025836 (2023).
30. Svensson, S. L. & Chao, Y. RNase III-CLASH brings bacterial RNA networks into focus. *Trends Microbiol.* **30**, 1125–1127 (2022).
31. Melamed, S. et al. Global mapping of small RNA-target interactions in bacteria. *Mol. Cell* **63**, 884–897 (2016).
32. Iosub, I. A. et al. Hfq CLASH uncovers sRNA-target interaction networks linked to nutrient availability adaptation. *Elife* **9**, e54655 (2020).
33. Sittka, A., Pfeiffer, V., Tedin, K. & Vogel, J. The RNA chaperone Hfq is essential for the virulence of Salmonella typhimurium. *Mol. Microbiol* **63**, 193–217 (2007).
34. Liu, F. et al. In vivo RNA interactome profiling reveals 3'UTR-processed small RNA targeting a central regulatory hub. *Nat. Commun.* **14**, 8106 (2023).
35. Matera, G. et al. Global RNA interactome of Salmonella discovers a 5' UTR sponge for the MicF small RNA that connects membrane permeability to transport capacity. *Mol. Cell* **82**, 629–644.e4 (2022).
36. Gebhardt, M. J. et al. Hfq-licensed RNA-RNA interactome in Pseudomonas aeruginosa reveals a keystone sRNA. *Proc. Natl Acad. Sci. USA* **120**, e2218407120 (2023).
37. Huber M. et al. An RNA sponge controls quorum sensing dynamics and biofilm formation in Vibrio cholerae. *Nat. Commun.* **13**, 7585 (2022).
38. Fuchs, M. et al. A network of small RNAs regulates sporulation initiation in Clostridioides difficile. *EMBO J.* e112858. https://doi.org/10.15252/embj.2022112858 (2023).
39. Han, K., Tjaden, B. & Lory, S. GRIL-seq provides a method for identifying direct targets of bacterial small regulatory RNA by in vivo proximity ligation. *Nat. Microbiol.* **2**, 16239 (2016).
40. Sprenger, M., Siemers, M., Krautwurst, S. & Papenfort, K. Small RNAs direct attack and defense mechanisms in a quorum sensing phage and its host. *Cell Host Microbe* **32**, 727–738.e6 (2024).
41. Kim, W. & Lee, Y. Mechanism for coordinate regulation of rpoS by sRNA-sRNA interaction in Escherichia coli. *RNA Biol.* **17**, 176–187 (2020).
42. Papenfort, K. et al. Specific and pleiotropic patterns of mRNA regulation by ArcZ, a conserved, Hfq-dependent small RNA. *Mol. Microbiol.* **74**, 139–158 (2009).
43. Corcoran, C. P. et al. Superfolder GFP reporters validate diverse new mRNA targets of the classic porin regulator, MicF RNA. *Mol. Microbiol.* **84**, 428–445 (2012).
44. Wu, K.-M. et al. Genome sequencing and comparative analysis of Klebsiella pneumoniae NTUH-K2044, a strain causing liver abscess and meningitis. *J. Bacteriol.* **191**, 4492–4501 (2009).
45. Chao, Y. et al. In vivo cleavage map illuminates the central role of RNase E in coding and non-coding RNA pathways. *Mol. Cell* **65**, 39–51 (2017).
46. Dubois, Q. et al. Function and mechanism of action of the small regulatory RNA ArcZ in Enterobacterales. *RNA* rna.080010.124 https://doi.org/10.1261/rna.080010.124 (2024).
47. Abellón-Ruiz, J. et al. Structural basis for maintenance of bacterial outer membrane lipid asymmetry. *Nat. Microbiol.* **2**, 1616–1623 (2017).
48. Guest, R. L., Lee, M. J., Wang, W. & Silhavy, T. J. A periplasmic phospholipase that maintains outer membrane lipid asymmetry in Pseudomonas aeruginosa. *Proc. Natl Acad. Sci. USA* **120**, e2302546120 (2023).
49. Kelley-Loughnane, N. et al. Purification, kinetic studies, and homology model of Escherichia coli fructose-1,6-bisphosphatase. *Biochim. Biophys. Acta* **1594**, 6–16 (2002).
50. Mann, M., Wright, P. R. & Backofen, R. IntaRNA 2.0: enhanced and customizable prediction of RNA-RNA interactions. *Nucleic Acids Res.* **45**, W435–W439 (2017).
51. Rehmsmeier, M., Steffen, P., Höchsmann, M. & Giegerich, R. Fast and effective prediction of microRNA/target duplexes. *RNA* **10**, 1507–1517 (2004).
52. Palacios, M. et al. Identification of two regulators of virulence that are conserved in Klebsiella pneumoniae classical and hypervirulent strains. *mBio* **9**, e01443-18 (2018).
53. Malinverni, J. C. & Silhavy, T. J. An ABC transport system that maintains lipid asymmetry in the Gram-negative outer membrane. *Proc. Natl Acad. Sci. USA* **106**, 8009–8014 (2009).
54. Sutterlin, H. A. et al. Disruption of lipid homeostasis in the Gram-negative cell envelope activates a novel cell death pathway. *Proc. Natl Acad. Sci. USA* **113**, E1565–E1574 (2016).
55. Tang, X. et al. Structural insights into outer membrane asymmetry maintenance in Gram-negative bacteria by MlaFEDB. *Nat. Struct. Mol. Biol.* **28**, 81–91 (2021).
56. Yeow, J., Luo, M. & Chng, S.-S. Molecular mechanism of phospholipid transport at the bacterial outer membrane interface. *Nat. Commun.* **14**, 8285 (2023).
57. Mandin, P. & Gottesman, S. Integrating anaerobic/aerobic sensing and the general stress response through the ArcZ small RNA. *EMBO J.* **29**, 3094–3107 (2010).

58. Chu, W. H. W. et al. Acquisition of regulator on virulence plasmid of hypervirulent Klebsiella allows bacterial lifestyle switch in response to iron. *mBio* **0**, e01297–23 (2023).
59. Ernst, C. M. et al. Adaptive evolution of virulence and persistence in carbapenem-resistant Klebsiella pneumoniae. *Nat. Med.* **26**, 705–711 (2020).
60. Khadka, S. et al. Urine-mediated suppression of Klebsiella pneumoniae mucoidy is counteracted by spontaneous Wzc variants altering capsule chain length. *mSphere* **0**, e00288–23 (2023).
61. Chao, Y., Papenfort, K., Reinhardt, R., Sharma, C. M. & Vogel, J. An atlas of Hfq-bound transcripts reveals 3′ UTRs as a genomic reservoir of regulatory small RNAs. *EMBO J.* **31**, 4005–4019 (2012).
62. Ruhland, E. et al. The global RNA-RNA interactome of Klebsiella pneumoniae unveils a small RNA regulator of cell division. *Proc. Natl Acad. Sci. USA* **121**, e2317322121 (2024).
63. Goh, K. J. et al. RIL-seq reveals extensive involvement of small RNAs in virulence and capsule regulation in hypervirulent Klebsiella pneumoniae. *Nucleic Acids Res.* gkae440 https://doi.org/10.1093/nar/gkae440 (2024).
64. Melamed, S. et al. Mapping the small RNA interactome in bacteria using RIL-seq. *Nat. Protoc.* **13**, 1–33 (2018).
65. Chao, Y. & Vogel, J. A 3′ UTR-derived small RNA provides the regulatory noncoding arm of the inner membrane stress response. *Mol. Cell* **61**, 352–363 (2016).
66. Moon, K. & Gottesman, S. A PhoQ/P-regulated small RNA regulates sensitivity of Escherichia coli to antimicrobial peptides. *Mol. Microbiol.* **74**, 1314–1330 (2009).
67. Yin, X. et al. The small protein MgtS and small RNA MgrR modulate the PitA phosphate symporter to boost intracellular magnesium levels. *Mol. Microbiol.* **111**, 131–144 (2019).
68. Sedlyarova, N. et al. sRNA-mediated control of transcription termination in E. coli. *Cell* **167**, 111–121.e13 (2016).
69. Neubacher, N. et al. Symbiosis, virulence and natural-product biosynthesis in entomopathogenic bacteria are regulated by a small RNA. *Nat. Microbiol* **5**, 1481–1489 (2020).
70. Lin, D. et al. The fructose-specific phosphotransferase system of Klebsiella pneumoniae is regulated by global regulator CRP and Linked to virulence and growth. *Infect. Immun.* **86**, e00340-18 (2018).
71. Beisel, C. L. & Storz, G. The base-pairing RNA spot 42 participates in a multioutput feedforward loop to help enact catabolite repression in Escherichia coli. *Mol. Cell* **41**, 286–297 (2011).
72. Papenfort, K. et al. Systematic deletion of Salmonella small RNA genes identifies CyaR, a conserved CRP-dependent riboregulator of OmpX synthesis. *Mol. Microbiol.* **68**, 890–906 (2008).
73. Beisel, C. L. & Storz, G. Base pairing small RNAs and their roles in global regulatory networks. *FEMS Microbiol. Rev.* **34**, 866–882 (2010).
74. Popella, L. et al. Global RNA profiles show target selectivity and physiological effects of peptide-delivered antisense antibiotics. *Nucleic Acids Res.* **49**, 4705–4724 (2021).
75. Vogel, J. An RNA biology perspective on species-specific programmable RNA antibiotics. *Mol. Microbiol.* **113**, 550–559 (2020).
76. Huang, T.-W. et al. Capsule deletion via a λ-Red knockout system perturbs biofilm formation and fimbriae expression in Klebsiella pneumoniae MGH 78578. *BMC Res. Notes* **7**, 13 (2014).
77. Uzzau, S., Figueroa-Bossi, N., Rubino, S. & Bossi, L. Epitope tagging of chromosomal genes in Salmonella. *Proc. Natl Acad. Sci. USA* **98**, 15264–15269 (2001).
78. Westermann, A. J. et al. Dual RNA-seq unveils noncoding RNA functions in host-pathogen interactions. *Nature* **529**, 496–501 (2016).

Acknowledgements

We are grateful to Drs. Joan Mecsas, Francesca Short, Hong-Yu Ou, Min Li, and Chao Yang for providing *Klebsiella* strains, Dr. Yunn-Hwen Gan for discussion. This study was financially supported by the National Key R&D Program of China (2022YFE0111800 and 2022YFC2303200 to Y.C.), the Chinese Academy of Sciences (XDB0570000 and 176002GJHZ2022022MI to Y.C.), the Natural Science Foundation of China (32270064 to Y.C., 32200031 to K.W.), Shanghai Municipal Science and Technology Commission (21ZR1471300 and 2019SHZDZX02 to Y.C.), and Shanghai Super Postdoc Fellowship (R.D).

Author contributions

Y.C. designed the study; K.W. and X.L. performed iRIL-seq analysis; K.W. characterized ArcZ and mechanisms of target regulation; X.L. performed capsule quantifications, characterized regulation by CRP and molecular function of MlaA; Y.L. analyzed clinical isolates and performed mice infection experiments with help from R.D. and H.J.; J.Z., N.S. contributed materials and regents; K.W. processed RNA-seq data; K.W., X.L., S.L.S., Y.C. analyzed results; S.L.S., A.C., Y.C. revised manuscript; Y.C. wrote the manuscript, supervised the project and secured funding.

Competing interests

The authors declare no competing interests.

Additional information

Supplementary information The online version contains supplementary material available at https://doi.org/10.1038/s41467-024-51213-z.

Correspondence and requests for materials should be addressed to Yanjie Chao.

Peer review information *Nature Communications* thanks Jorgen Johansson, and the other, anonymous, reviewer(s) for their contribution to the peer review of this work. A peer review file is available.